

FULL WAVEFORM INVERSION OF VISCOELASTIC MEDIUM BASED ON GRADIENT PREPROCESSING

YIPENG XU^{1,2,3}, KAI ZHANG^{1,2}, ZHENCHUN LI^{1,2}, ZILIN HE^{1,2,3},
JICHUAN WANG^{1,2} and JINFENG GAO^{1,2}

¹ SWPI, School of Geosciences, China University of Petroleum (East China), Qingdao 266580, P.R. China. xyp1759029715@163.com

² Shandong Provincial Key Laboratory of Deep Oil & Gas, China University of Petroleum (East China), Qingdao 266580, P.R. China.

³ Geophysical Research Institute of Sinopec Shengli Oilfield Corporation, Dongying 257022, P.R. China.

(Received March 18, 2022; accepted September 21, 2022)

ABSTRACT

Xu, Y.P., Zhang, K., Li, Z.C., He, Z.L., Wang, J.C. and Gao, J.F., 2022. Full waveform inversion of viscoelastic medium based on gradient preprocessing. *Journal of Seismic Exploration*, 31: 579-596.

The subsurface medium exists mainly in a viscoelastic form, and there are two phenomena: amplitude attenuation and phase dispersion. However, the full waveform inversion is used to inverse the subsurface medium parameters in a large scale way, and the phase dispersion phenomenon is more often solved by migration. Therefore, we investigate the Kelvin-Voigt model with only amplitude attenuation. In this paper, we derive the back propagation wavefield formulation and gradient formulation for full waveform inversion of viscoelastic media based on the Kelvin-Voigt model, and analyze the correctness and feasibility of the method. Also, in viscoelastic media, low velocity geological bodies may cause the gradient of the full waveform inversion to fall into local convergence. It is shown that the gradient preprocessing method based on the pseudo-Hessian operator can suppress the gradient from falling into local convergence. Therefore, this manuscript incorporates a pseudo-Hessian operator for gradient preprocessing and derives a gradient preprocessing formulation for full waveform inversion of viscoelastic media based on gradient preprocessing, which solves the problem that the inversion gradient falls into local convergence. It is demonstrated through examples that the method can solve the problem of the inversion gradient falling into local convergence caused by the low-velocity body in the full waveform inversion of viscoelastic media.

KEY WORDS: viscoelastic media, gradient preprocessing, Kelvin-Voigt model, full waveform inversion.

INTRODUCTION

Among multi-parameter seismic inversions, full waveform inversion (FWI) is a high-precision inversion method (Tarantola, 1984; Pratt et al., 1999; Mora, 1987) with the potential to provide accurate parametric models of the subsurface medium. And now the full waveform inversion has been mainly studied with viscous acoustic media (Ren et al, 2015; Yong et al, 2021). However, purely elastic and viscous acoustic media do not exist in the subsurface medium, but more in the form of viscoelastic media. In addition, there are two phenomena of amplitude attenuation and phase dispersion in viscoelastic media. However, the full waveform inversion is used to inverse the subsurface medium parameters in a large scale way, and the phase dispersion phenomenon is more often solved by migration. Therefore, we investigate the Kelvin-Voigt model with only amplitude attenuation. In this paper, we derive the back propagation wavefield formulation and gradient formulation for full waveform inversion of viscoelastic media based on the Kelvin-Voigt model, and analyze the correctness and feasibility of the method.

Also, in viscoelastic media, low velocity geological bodies may cause the gradient of the full waveform inversion to fall into local convergence. The problem of how to suppress the gradient from falling into local convergence in the full waveform inversion of viscoelastic media needs to be solved urgently. Wang et al. (2017) analyzed the Hessian matrix and resolution matrix using the method of decoupling the P- and S- waves of the second-order elastic wave equation, and confirmed that the conjugate gradient preprocessing of the P- and S- wave separation can effectively suppress the crosstalk effects and improve the accuracy of the inversion of the low-velocity anomalies. Chen et al. (2017) derive the pseudo-Hessian matrix of each isoelastic wave for gradient preprocessing.

The above study shows that the gradient preprocessing method based on the pseudo-Hessian operator can suppress the gradient from falling into local convergence. Therefore, in this paper, we incorporate the pseudo-Hessian operator for gradient preprocessing and derive a gradient preprocessing formulation based on gradient preprocessing for full waveform inversion of viscoelastic media (referred to as P-QEFWI), which solves the problem that the inversion gradient falls into local convergence. It is demonstrated through examples that the method can solve the problem of the inversion gradient falling into local convergence caused by the low-velocity body in the full waveform inversion of viscoelastic media (referred to as QEFWI).

PRINCIPLE OF FULL WAVEFORM INVERSION FOR VISCOELASTIC MEDIA BASED ON GRADIENT PREPROCESSING

In this paper, we derive the equation for the Kelvin-Voigt model, and the isotropic wavefield equation for a viscoelastic medium based on the Kelvin-Voigt model is as follows (Fu et al., 1993; Ren et al., 2014)

$$\left\{ \begin{array}{l} \rho \frac{\partial u_x}{\partial t} = \frac{\partial \tau_{xx}}{\partial x} + \frac{\partial \tau_{xz}}{\partial z} \\ \rho \frac{\partial u_z}{\partial t} = \frac{\partial \tau_{xz}}{\partial x} + \frac{\partial \tau_{zz}}{\partial z} \\ \frac{\partial \tau_{xx}}{\partial t} = (\lambda + 2\mu) \frac{\partial u_x}{\partial x} + \lambda \frac{\partial u_z}{\partial z} + (\lambda' + 2\mu') \frac{\partial}{\partial x} \left(\frac{\partial u_x}{\partial t} \right) + \lambda' \frac{\partial}{\partial z} \left(\frac{\partial u_z}{\partial t} \right) \\ \frac{\partial \tau_{zz}}{\partial t} = (\lambda + 2\mu) \frac{\partial u_z}{\partial z} + \lambda \frac{\partial u_x}{\partial x} + (\lambda' + 2\mu') \frac{\partial}{\partial z} \left(\frac{\partial u_z}{\partial t} \right) + \lambda' \frac{\partial}{\partial x} \left(\frac{\partial u_x}{\partial t} \right) \\ \frac{\partial \tau_{xz}}{\partial t} = \mu \left(\frac{\partial u_x}{\partial z} + \frac{\partial u_z}{\partial x} \right) + \mu' \left(\frac{\partial}{\partial z} \left(\frac{\partial u_x}{\partial t} \right) + \frac{\partial}{\partial x} \left(\frac{\partial u_z}{\partial t} \right) \right) \end{array} \right. \quad (1)$$

$(u_x, u_z, \tau_{xx}, \tau_{zz}, \tau_{xz})$ is the wave field component and $\left(\frac{\partial u_x}{\partial t}, \frac{\partial u_z}{\partial t}\right)$ is the memory variable of the viscoelastic wave field component. $(\lambda, \mu, \lambda', \mu')$ are the Lamé coefficients. Some variables in eq. (1) can be expressed as the following equation

$$\left\{ \begin{array}{l} \lambda + 2\mu = \rho V_p^2, \lambda' + 2\mu' = \frac{\rho V_p^2}{Q_p 2\pi f_0} \\ \mu = \rho V_s^2, \mu' = \frac{\rho V_s^2}{Q_s 2\pi f_0} \\ \lambda = \rho V_p^2 - 2\rho V_s^2, \lambda' = \frac{\rho V_p^2}{Q_p 2\pi f_0} - 2 \frac{\rho V_s^2}{Q_s 2\pi f_0} \\ \omega = 2\pi f_0 \end{array} \right. \quad (2)$$

V_p is the longitudinal propagation velocity of the P-wave in the subsurface medium, V_s is the longitudinal propagation velocity of the S-wave in the subsurface medium, and ρ is the density. f_0 is the main frequency of the seismic subwave, and (Q_p, Q_s) is the quality factor of the longitudinal and transverse waves. The objective function of the full waveform inversion in elastic waves can be written as the following equation

$$\min \mathbf{E}(v) = \frac{1}{2} \int_0^T \|d_{calx} - d_{obsx}\|^2 + \|d_{calz} - d_{obsz}\|^2 dt, \quad (3)$$

\mathbf{E} is the objective function, (d_{calx}, d_{calz}) is the simulated seismic record, and (d_{obsx}, d_{obsz}) is the observed seismic record. According to the adjoint state method, we use Lagrange multipliers to modify the objective function as

$$\begin{aligned} \min \mathbf{E}(v) = & \int_0^T [\|d_{calx} - d_{obsx}\|^2 + \|d_{calz} - d_{obsz}\|^2] dt \\ & + \int_0^T (\Lambda_1 N_1 + \Lambda_2 N_2 + \Lambda_3 N_3 + \Lambda_4 N_4 + \Lambda_5 N_5) dt, \end{aligned} \quad (4)$$

Λ_i , ($i=1,2,\dots,5$) are Lagrange multipliers and H_i , ($i = 1,2,\dots,5$) are the corresponding first-order velocity stress equations as follows

$$\left\{ \begin{array}{l} N_1 = \rho \frac{\partial u_x}{\partial t} - \frac{\partial \tau_{xx}}{\partial x} - \frac{\partial \tau_{xz}}{\partial z} \\ N_2 = \rho \frac{\partial u_z}{\partial t} - \frac{\partial \tau_{xz}}{\partial x} - \frac{\partial \tau_{zz}}{\partial z} \\ N_3 = \frac{\partial \tau_{xx}}{\partial t} - (\lambda + 2\mu) \frac{\partial u_x}{\partial x} - \lambda \frac{\partial u_z}{\partial z} - (\lambda' + 2\mu') \frac{\partial}{\partial x} \left(\frac{\partial u_x}{\partial t} \right) - \lambda' \frac{\partial}{\partial z} \left(\frac{\partial u_z}{\partial t} \right) \\ N_4 = \frac{\partial \tau_{zz}}{\partial t} - (\lambda + 2\mu) \frac{\partial u_z}{\partial z} - \lambda \frac{\partial u_x}{\partial x} - (\lambda' + 2\mu') \frac{\partial}{\partial z} \left(\frac{\partial u_z}{\partial t} \right) - \lambda' \frac{\partial}{\partial x} \left(\frac{\partial u_x}{\partial t} \right) \\ N_5 = \frac{\partial \tau_{xz}}{\partial t} - \mu \left(\frac{\partial u_x}{\partial z} + \frac{\partial u_z}{\partial x} \right) - \mu' \left(\frac{\partial}{\partial z} \left(\frac{\partial u_x}{\partial t} \right) + \frac{\partial}{\partial x} \left(\frac{\partial u_z}{\partial t} \right) \right) \end{array} \right. \quad (5)$$

We take derivatives for each component in eq. (4)

$$\begin{aligned} \frac{\partial E(v)}{\partial u_{calx}} \vartheta u_{calx} &= \int_0^T [\|d_{calx} - d_{obsx}\|^2] dt \\ &+ \int_0^T \left[\begin{array}{l} \Lambda_1 \rho \frac{\partial u_x}{\partial t} - \Lambda_3 (\lambda + 2\mu) \frac{\partial u_x}{\partial x} - \\ \Lambda_3 (\lambda' + 2\mu') \frac{\partial}{\partial x} \left(\frac{\partial u_x}{\partial t} \right) - \Lambda_4 \lambda \frac{\partial u_x}{\partial x} \\ -\Lambda_4 \lambda' \frac{\partial}{\partial x} \left(\frac{\partial u_x}{\partial t} \right) - \Lambda_5 \mu \frac{\partial u_x}{\partial z} - \Lambda_5 \mu' \frac{\partial}{\partial z} \left(\frac{\partial u_x}{\partial t} \right) \end{array} \right] dt \end{aligned} \quad (6-1)$$

$$\begin{aligned} \frac{\partial E(v)}{\partial u_{calz}} \vartheta u_{calz} &= \int_0^T [\|d_{calz} - d_{obsz}\|^2] dt \\ &+ \int_0^T \left[\begin{array}{l} \Lambda_2 \rho \frac{\partial u_z}{\partial t} - \Lambda_3 \lambda \frac{\partial u_z}{\partial z} - \Lambda_3 \lambda' \frac{\partial}{\partial z} \left(\frac{\partial u_z}{\partial t} \right) \\ -\Lambda_4 (\lambda + 2\mu) \frac{\partial u_z}{\partial z} - \Lambda_4 (\lambda' + 2\mu') \frac{\partial}{\partial z} \left(\frac{\partial u_z}{\partial t} \right) \\ -\Lambda_5 \mu \frac{\partial u_z}{\partial x} - \Lambda_5 \mu' \frac{\partial}{\partial x} \left(\frac{\partial u_z}{\partial t} \right) \end{array} \right] dt \end{aligned} \quad (6-2)$$

$$\frac{\partial E(v)}{\partial \tau_{xx}} \vartheta \tau_{xx} = \int_0^T \left[-\Lambda_1 \frac{\partial \tau_{xx}}{\partial x} + \Lambda_3 \frac{\partial \tau_{xx}}{\partial t} \right] dt \quad (6-3)$$

$$\frac{\partial E(v)}{\partial \tau_{zz}} \vartheta \tau_{zz} = \int_0^T \left[-\Lambda_2 \frac{\partial \tau_{zz}}{\partial z} + \Lambda_4 \frac{\partial \tau_{zz}}{\partial t} \right] dt \quad (6-4)$$

$$\frac{\partial E(v)}{\partial \tau_{xz}} \vartheta \tau_{xz} = \int_0^T \left[-\Lambda_1 \frac{\partial \tau_{xz}}{\partial z} - \Lambda_2 \frac{\partial \tau_{xz}}{\partial x} + \Lambda_5 \frac{\partial \tau_{xz}}{\partial t} \right] dt \quad (6-5)$$

We organize eq. (6) by replacing the Lagrangian multipliers by the original variables with "*", and we obtain the back propagation wave field equation:

$$\left\{ \begin{array}{l}
\rho \frac{\partial u_x^*}{\partial t} = (\lambda + 2\mu) \frac{\partial \tau_{xx}^*}{\partial x} + (\lambda' + 2\mu') \frac{\partial}{\partial x} \left(\frac{\partial u_x^*}{\partial t} \right) + \lambda \frac{\partial \tau_{zz}^*}{\partial x} + \\
\lambda' \frac{\partial}{\partial x} \left(\frac{\partial u_x^*}{\partial t} \right) + \mu \frac{\partial \tau_{xz}^*}{\partial z} + \mu' \frac{\partial}{\partial z} \left(\frac{\partial u_x^*}{\partial t} \right) + (d_{calx} - d_{obsx}) \\
\rho \frac{\partial u_z^*}{\partial t} = \lambda \frac{\partial \tau_{xx}^*}{\partial z} + \lambda' \frac{\partial}{\partial z} \left(\frac{\partial u_z^*}{\partial t} \right) + (\lambda + 2\mu) \frac{\partial u_z^*}{\partial z} + (\lambda' + 2\mu') \frac{\partial}{\partial z} \left(\frac{\partial u_z^*}{\partial t} \right) \\
+ \mu \frac{\partial \tau_{xz}^*}{\partial x} + \mu' \frac{\partial}{\partial x} \left(\frac{\partial u_z^*}{\partial t} \right) + (d_{calz} - d_{obsz}) \\
\frac{\partial \tau_{xx}^*}{\partial t} = \frac{\partial u_x^*}{\partial x} \\
\frac{\partial \tau_{zz}^*}{\partial t} = \frac{\partial u_z^*}{\partial z} \\
\frac{\partial \tau_{xz}^*}{\partial t} = \frac{\partial u_x^*}{\partial z} + \frac{\partial u_z^*}{\partial x}
\end{array} \right. \quad (7)$$

The upper right corner with "*" is the variable of the back propagation wave field. Next, we take the parameter perturbation term of the wave equation as follows

$$\left\{ \begin{array}{l}
(\rho + \vartheta\rho) \frac{\partial(u_x + \vartheta u_x)}{\partial t} = \frac{\partial(\tau_{xx} + \vartheta\tau_{xx})}{\partial x} + \frac{\partial(\tau_{xz} + \vartheta\tau_{xz})}{\partial z} \\
(\rho + \vartheta\rho) \frac{\partial(u_z + \vartheta u_z)}{\partial t} = \frac{\partial(\tau_{xz} + \vartheta\tau_{xz})}{\partial x} + \frac{\partial(\tau_{zz} + \vartheta\tau_{zz})}{\partial z} \\
\frac{\partial(\tau_{xx} + \vartheta\tau_{xx})}{\partial t} = (\lambda + 2\mu + \vartheta\lambda + 2\vartheta\mu) \frac{\partial(u_x + \vartheta u_x)}{\partial x} + (\lambda + \vartheta\lambda) \frac{\partial(u_z + \vartheta u_z)}{\partial z} \\
+ (\lambda' + 2\mu' + \vartheta\lambda' + 2\vartheta\mu') \frac{\partial}{\partial x} \left(\frac{\partial u_x}{\partial t} + \vartheta \frac{\partial u_x}{\partial t} \right) + (\lambda' + \vartheta\lambda') \frac{\partial}{\partial z} \left(\frac{\partial u_z}{\partial t} + \vartheta \frac{\partial u_z}{\partial t} \right) \\
\frac{\partial(\tau_{zz} + \vartheta\tau_{zz})}{\partial t} = (\lambda + 2\mu + \vartheta\lambda + 2\vartheta\mu) \frac{\partial(u_z + \vartheta u_z)}{\partial z} + (\lambda + \vartheta\lambda) \frac{\partial(u_x + \vartheta u_x)}{\partial x} \\
+ (\lambda' + 2\mu' + \vartheta\lambda' + 2\vartheta\mu') \frac{\partial}{\partial z} \left(\frac{\partial u_z}{\partial t} + \vartheta \frac{\partial u_z}{\partial t} \right) + (\lambda' + \vartheta\lambda') \frac{\partial}{\partial x} \left(\frac{\partial u_x}{\partial t} + \vartheta \frac{\partial u_x}{\partial t} \right) \\
\frac{\partial \tau_{xz}}{\partial t} = (\mu + \vartheta\mu) \left(\frac{\partial(u_x + \vartheta u_x)}{\partial z} + \frac{\partial(u_z + \vartheta u_z)}{\partial x} \right) \\
+ (\mu' + \vartheta\mu') \left(\frac{\partial}{\partial z} \left(\frac{\partial u_x}{\partial t} + \vartheta \frac{\partial u_x}{\partial t} \right) + \frac{\partial}{\partial x} \left(\frac{\partial u_z}{\partial t} + \vartheta \frac{\partial u_z}{\partial t} \right) \right)
\end{array} \right. \quad (8)$$

We take the parameter perturbation term of eq. (8)

$$\vartheta \mathbf{E} = \begin{pmatrix} -\vartheta \rho \frac{\partial u_x}{\partial t} \\ -\vartheta \rho \frac{\partial u_z}{\partial t} \\ (\vartheta \lambda + 2\vartheta \mu) \frac{\partial u_x}{\partial x} + \vartheta \lambda \frac{\partial u_z}{\partial z} + (\vartheta \lambda' + 2\vartheta \mu') \frac{\partial}{\partial x} \left(\frac{\partial u_x}{\partial t} \right) + (\vartheta \lambda') \frac{\partial}{\partial z} \left(\frac{\partial u_z}{\partial t} \right) \\ (\vartheta \lambda + 2\vartheta \mu) \frac{\partial u_z}{\partial z} + \vartheta \lambda \frac{\partial u_x}{\partial x} + (\vartheta \lambda' + 2\vartheta \mu') \frac{\partial}{\partial z} \left(\frac{\partial u_z}{\partial t} \right) + (\vartheta \lambda') \frac{\partial}{\partial x} \left(\frac{\partial u_x}{\partial t} \right) \\ \vartheta \mu \left(\frac{\partial (u_x)}{\partial z} + \frac{\partial (u_z)}{\partial x} \right) + \vartheta \mu' \left(\frac{\partial}{\partial z} \left(\frac{\partial u_x}{\partial t} \right) + \frac{\partial}{\partial x} \left(\frac{\partial u_z}{\partial t} \right) \right) \end{pmatrix} \begin{pmatrix} u_x^* \\ u_z^* \\ \tau_{xx}^* \\ \tau_{zz}^* \\ \tau_{xz}^* \end{pmatrix}^T \quad (9)$$

We compute the matrix as follows

$$\begin{aligned} \vartheta \mathbf{E} = & \vartheta \rho \frac{\partial u_x}{\partial t} u_x^* + \vartheta \rho \frac{\partial u_z}{\partial t} u_z^* + \tau_{xx}^* \left((\vartheta \lambda + 2\vartheta \mu) \frac{\partial u_x}{\partial x} + \vartheta \lambda \frac{\partial u_z}{\partial z} + (\vartheta \lambda' + \right. \\ & \left. 2\vartheta \mu') \frac{\partial}{\partial x} \left(\frac{\partial u_x}{\partial t} \right) + (\vartheta \lambda') \frac{\partial}{\partial z} \left(\frac{\partial u_z}{\partial t} \right) \right) + \tau_{zz}^* \left((\vartheta \lambda + 2\vartheta \mu) \frac{\partial u_z}{\partial z} + \vartheta \lambda \frac{\partial u_x}{\partial x} + \right. \\ & \left. (\vartheta \lambda' + 2\vartheta \mu') \frac{\partial}{\partial z} \left(\frac{\partial u_z}{\partial t} \right) + (\vartheta \lambda') \frac{\partial}{\partial x} \left(\frac{\partial u_x}{\partial t} \right) \right) + \tau_{xz}^* \left(\vartheta \mu \left(\frac{\partial (u_x)}{\partial z} + \frac{\partial (u_z)}{\partial x} \right) + \right. \\ & \left. \vartheta \mu' \left(\frac{\partial}{\partial z} \left(\frac{\partial u_x}{\partial t} \right) + \frac{\partial}{\partial x} \left(\frac{\partial u_z}{\partial t} \right) \right) \right) \end{aligned} \quad (10)$$

We partial derivate the parameters and obtain the gradient equation as follows

$$\left\{ \begin{aligned} \frac{\partial \mathbf{E}}{\partial \rho} &= - \int_0^T \frac{\partial u_x}{\partial t} u_x^* + \frac{\partial u_z}{\partial t} u_z^* dt \\ \frac{\partial \mathbf{E}}{\partial \lambda} &= \int_0^T (\tau_{xx}^* + \tau_{zz}^*) \left(\frac{\partial u_x}{\partial x} + \frac{\partial u_z}{\partial z} \right) dt \\ \frac{\partial \mathbf{E}}{\partial \mu} &= \int_0^T 2 \left(\tau_{xx}^* \frac{\partial u_x}{\partial x} + \tau_{zz}^* \frac{\partial u_z}{\partial z} \right) + \tau_{xz}^* \left(\frac{\partial u_x}{\partial z} + \frac{\partial u_z}{\partial x} \right) dt \\ \frac{\partial \mathbf{E}}{\partial \lambda'} &= \int_0^T (\tau_{xx}^* + \tau_{zz}^*) \left(\frac{\partial}{\partial x} \left(\frac{\partial u_x}{\partial t} \right) + \frac{\partial}{\partial z} \left(\frac{\partial u_z}{\partial t} \right) \right) dt \\ \frac{\partial \mathbf{E}}{\partial \mu'} &= \int_0^T 2 \left(\frac{\partial}{\partial x} \left(\frac{\partial u_x}{\partial t} \right) \tau_{xx}^* + \frac{\partial}{\partial z} \left(\frac{\partial u_z}{\partial t} \right) \tau_{zz}^* \right) + \tau_{xz}^* \left(\frac{\partial}{\partial z} \left(\frac{\partial u_x}{\partial t} \right) + \frac{\partial}{\partial x} \left(\frac{\partial u_z}{\partial t} \right) \right) dt \end{aligned} \right. \quad (11)$$

The chain rule leads to the following:

$$\left\{ \begin{array}{l} \frac{\partial E}{\partial V_p} = 2\rho V_p \frac{\partial E}{\partial \lambda} + \frac{\rho V_p}{Q_p \pi f_0} \frac{\partial E}{\partial \lambda'} \\ \frac{\partial E}{\partial V_s} = -4\rho V_s \frac{\partial E}{\partial \lambda} + 2\rho V_s \frac{\partial E}{\partial \mu} - \frac{2\rho V_s}{Q_s \pi f_0} \frac{\partial E}{\partial \lambda'} + \frac{\rho V_s}{Q_s \pi f_0} \frac{\partial E}{\partial \mu'} \\ \frac{\partial E}{\partial Q_p} = -\frac{\rho V_p^2}{Q_p^2 2\pi f_0} \frac{\partial E}{\partial \lambda'} \\ \frac{\partial E}{\partial Q_s} = \frac{\rho V_s^2}{Q_s^2 \pi f_0} \frac{\partial E}{\partial \lambda'} - \frac{\rho V_s^2}{Q_s^2 2\pi f_0} \frac{\partial E}{\partial \mu'} \end{array} \right. \quad (12)$$

In this paper, we next explain the gradient preprocessing method for full waveform inversion of viscoelastic media. In the case of considering only the Green function of the shot point without considering the Green function of the receiver point, the pseudo-Hessian operator is obtained as follows

$$\mathbf{H}_{pseudo} = \sum_i^{N_{shot}} \int \left(\frac{\partial \mathbf{L}}{\partial \mathbf{m}} \mathbf{u}_i \right)^T \left(\frac{\partial \mathbf{L}}{\partial \mathbf{m}} \mathbf{u}_i \right) \quad , \quad (13)$$

i is the number of shots, and \mathbf{u}_i is the wave field vector of the i -th shot. In this paper, the method is extended to a viscoelastic medium with the following equation

$$\left\{ \begin{array}{l} \mathbf{H}_\lambda = \sum_{shot} \int_0^T 2 \left(\frac{\partial(\tau_{xxa})}{\partial t} + \frac{\partial(\tau_{zza})}{\partial t} \right)^2 / (\lambda + 2\mu)^2 dt \\ \mathbf{H}_\mu = \sum_{shot} \int_0^T \left[\frac{\partial^2 \tau_{xza}}{\partial t^2} + \left(\frac{\partial(\tau_{xxa})}{\partial t} - \frac{\partial(\tau_{zza})}{\partial t} \right)^2 / 2\mu^2 + 2 \left(\frac{\partial(\tau_{xxa})}{\partial t} + \frac{\partial(\tau_{zza})}{\partial t} \right)^2 / (\lambda + 2\mu)^2 \right] dt \\ \mathbf{H}_{\lambda'} = \sum_{shot} \int_0^T \left(\frac{\partial(\tau_{xxq})}{\partial t} + \frac{\partial(\tau_{zzq})}{\partial t} \right)^2 / (2(\lambda' + 2\mu')^2) dt \\ \mathbf{H}_{\mu'} = \sum_{shot} \int_0^T \left[\frac{\partial^2 \tau_{xzq}}{\partial t^2} + \left(\frac{\partial(\tau_{xxq})}{\partial t} - \frac{\partial(\tau_{zzq})}{\partial t} \right)^2 / 2\mu'^2 + \left(\frac{\partial(\tau_{xxq})}{\partial t} + \frac{\partial(\tau_{zzq})}{\partial t} \right)^2 / (2(\lambda' + 2\mu')^2) \right] dt \end{array} \right. \quad (14)$$

$(\tau_{xxa}, \tau_{zza}, \tau_{xza})$ are the subvectors of the wavefield vector without viscous terms, and $(\tau_{xxq}, \tau_{zzq}, \tau_{xzq})$ are the vectors of viscous terms of the wavefield vector, both of which can be obtained directly in the forward motion. To prevent division by zero, a very small number α is added to the denominator in this paper. Therefore, the gradient preprocessing operator and the preprocessed gradient can be written as follows

$$\left\{ \begin{array}{l} \mathbf{P}_\lambda = 1/(\mathbf{H}_\lambda + \alpha) \\ \mathbf{P}_\mu = 1/(\mathbf{H}_\mu + \alpha) \\ \mathbf{P}_{\lambda'} = 1/(\mathbf{H}_{\lambda'} + \alpha) \\ \mathbf{P}_{\mu'} = 1/(\mathbf{H}_{\mu'} + \alpha) \end{array} \right\} \cdot \left\{ \begin{array}{l} \frac{\partial E}{\partial \lambda} = \mathbf{P}_\lambda \frac{\partial E}{\partial \lambda} \\ \frac{\partial E}{\partial \mu} = \mathbf{P}_\mu \frac{\partial E}{\partial \mu} \\ \frac{\partial E}{\partial \lambda'} = \mathbf{P}_{\lambda'} \frac{\partial E}{\partial \lambda'} \\ \frac{\partial E}{\partial \mu'} = \mathbf{P}_{\mu'} \frac{\partial E}{\partial \mu'} \end{array} \right. \quad . \quad (15)$$

Without rewriting the previous equations, eq. (15) can be directly substituted into the gradient equation. In the following, we will verify the method of this paper using the Sub-sag model and 2D BP gas chimney model.

EXAMPLES

In this paper, the correctness of the QEFWI method is tested using the Sub-sag model. The Sub-sag model (Fig. 1) size is 2000 m * 1000 m, space interval to 10 m. The source is the main frequency of 20 Hz Ricker wavelet, detector sampling interval is 1 ms, total sampling time of 1.20 s.

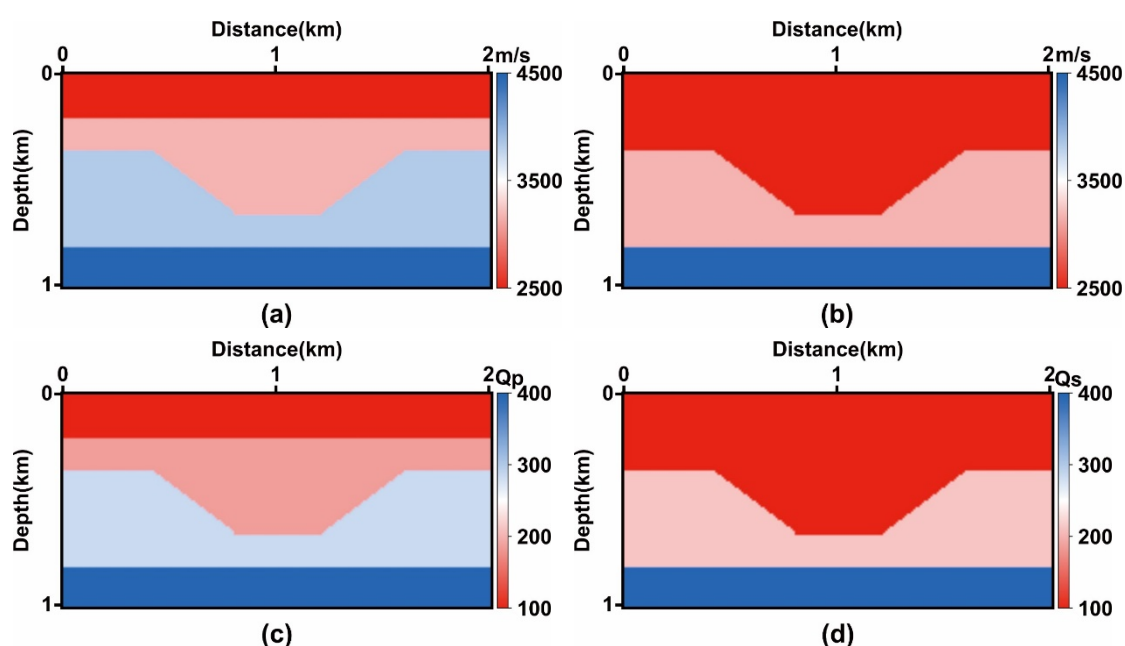


Fig. 1. Sub-sag model: (a) V_p , V_s (b), Q_p (c), Q_s (d)

In Fig. 2, the wave field of the viscoelastic medium exhibits a lower frequency as a result than the elastic wave field because the amplitude attenuation of the viscoelastic medium filters out the high-frequency components. In Fig. 3, the energy of a single-shot seismic record in a viscoelastic medium attenuates during propagation, but the position of the wave does not change, so there is only amplitude attenuation. This proves the correctness of the wave eq. (1).

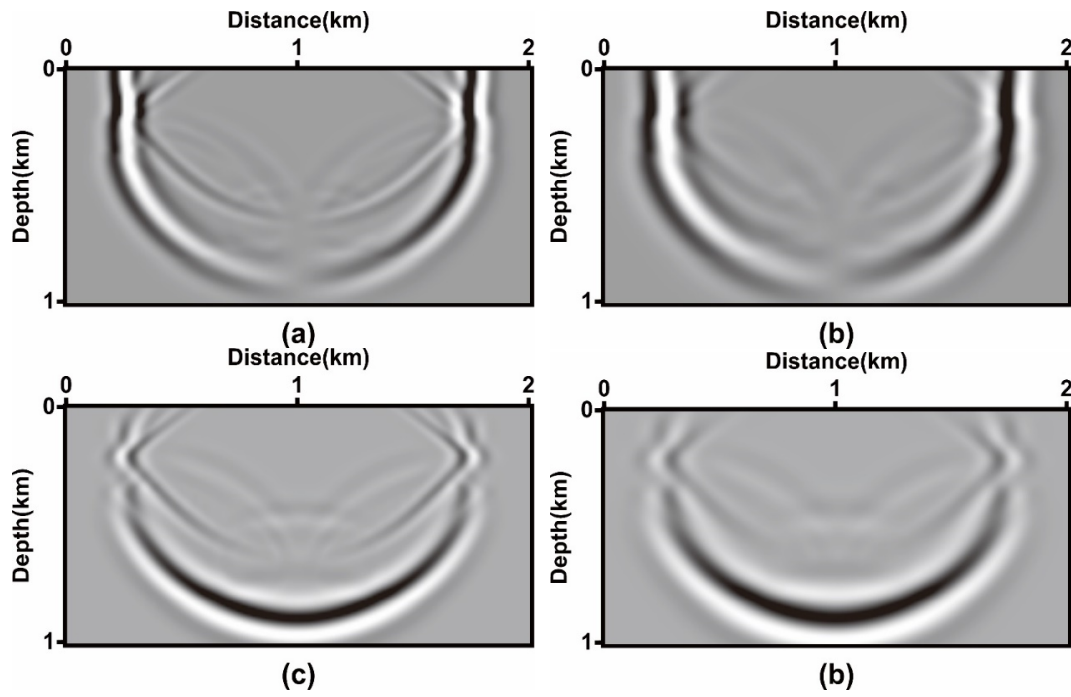


Fig. 2. Snapshot of wave field at 300 ms: (a) u_x component of elastic medium, (b) u_x component of viscoelastic medium, (c) u_z component of elastic medium, (d) u_z component of viscoelastic medium.

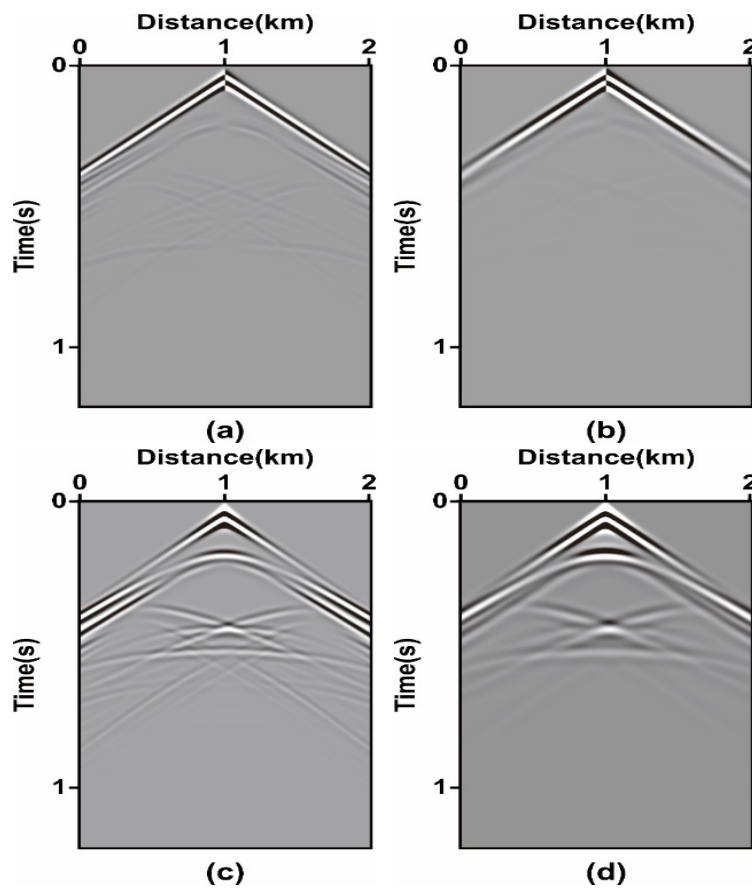


Fig. 3. Single-shot seismic records: (a) elastic medium u_x component, (b) viscoelastic medium u_x component, (c) elastic medium u_z component, (d) viscoelastic medium u_z component.

Fig. 4 shows the initial model used for the inversion. The update gradient of the full waveform inversion determines the results of the inversion, so we first compare the gradients. From Fig. 5, it can be obtained that the gradients of the four parameters match with the model, which proves the correctness of the gradient eqs. (11) and (12).

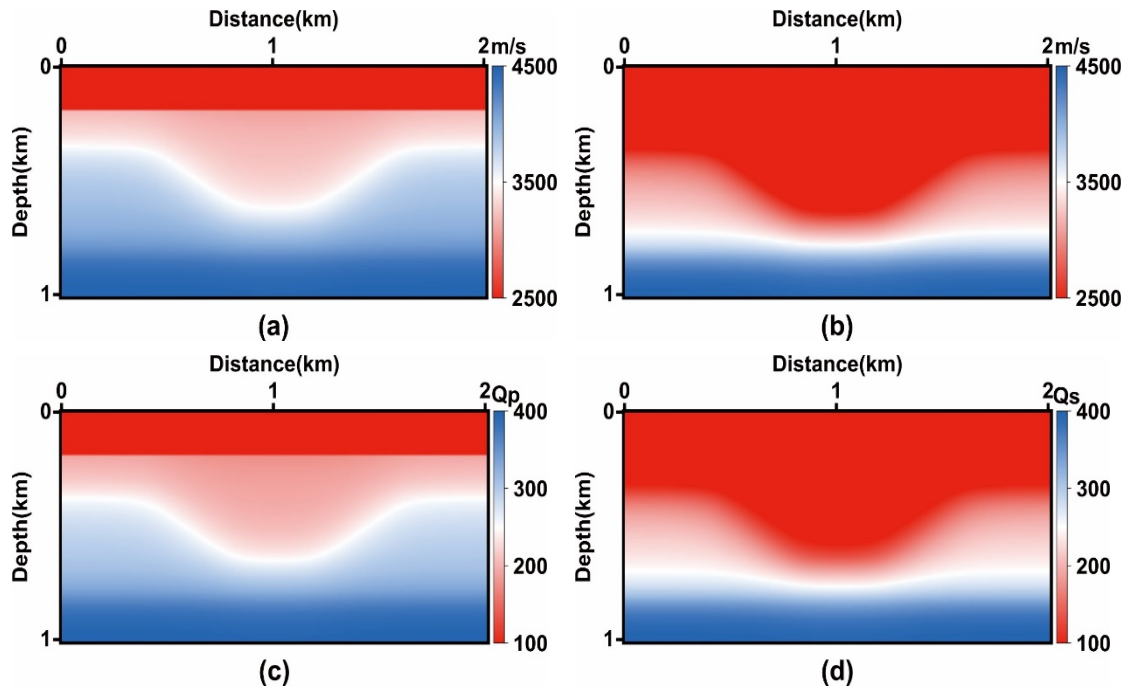


Fig. 4. Initial model: (a) V_p , (b) V_s , (c) Q_p , (d) Q_s .

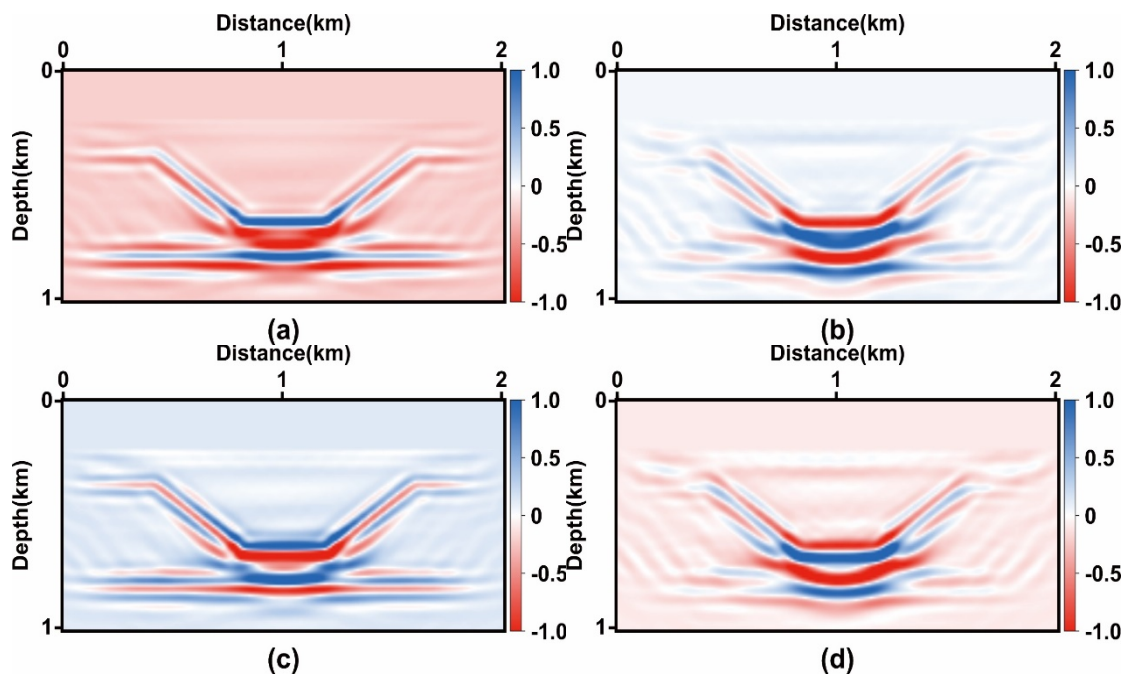


Fig. 5. Gradients: (a) V_p , (b) V_s , (c) Q_p , (d) Q_s

Next, we compare the inversion results of the Sub-sag model. As can be seen from Fig. 6, when the subsurface medium is not complex and the initial model is good, we obtain better inversion results for the parameters. In summary, the back propagation wavefield equation and gradient equation we derived for the full waveform inversion of viscoelastic media based on the Kelvin-Voigt model are correct.

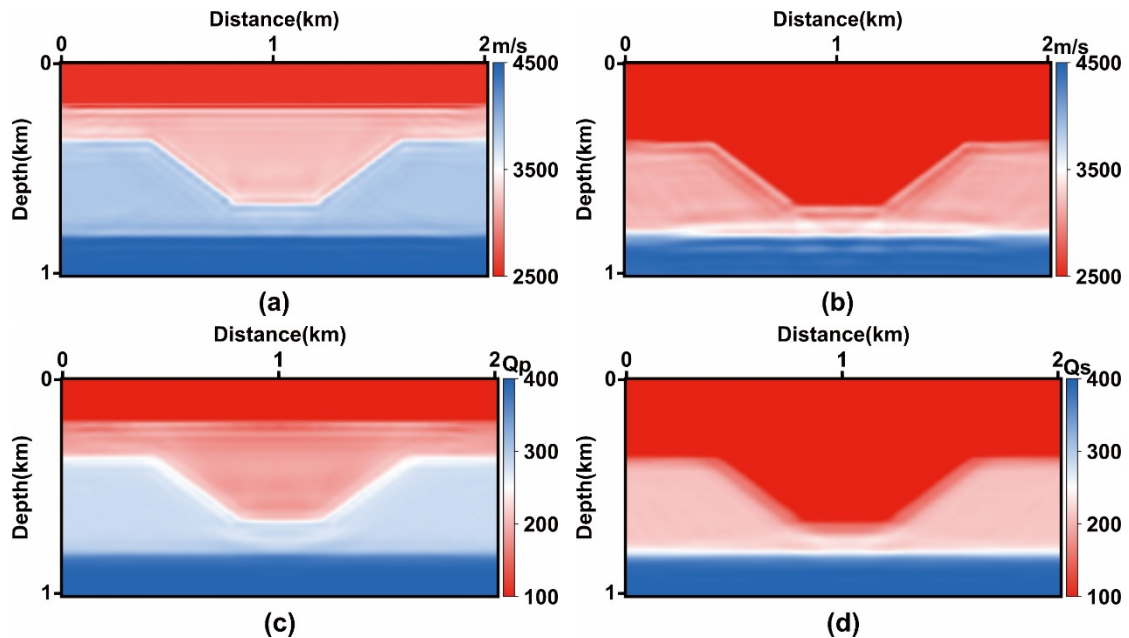


Fig. 6. Inversion results: (a) V_p , (b) V_s , (c) Q_p , (d) Q_s

In this paper, we test the effectiveness of the P-QEFWI method to suppress the gradient from falling into local convergence using a 2D BP gas chimney model. The top layer of the 2D BP gas chimney model (Fig. 7) has two low-velocity bodies with a size of $7,000 \text{ m} * 3,200 \text{ m}$ and a space interval of 10 m . The source is the main frequency of the 20 Hz Ricker wavelet, the detector sampling interval is 1 ms , and the total sampling time is 2.40 s . The initial model used for the inversion is shown in Fig. 8.

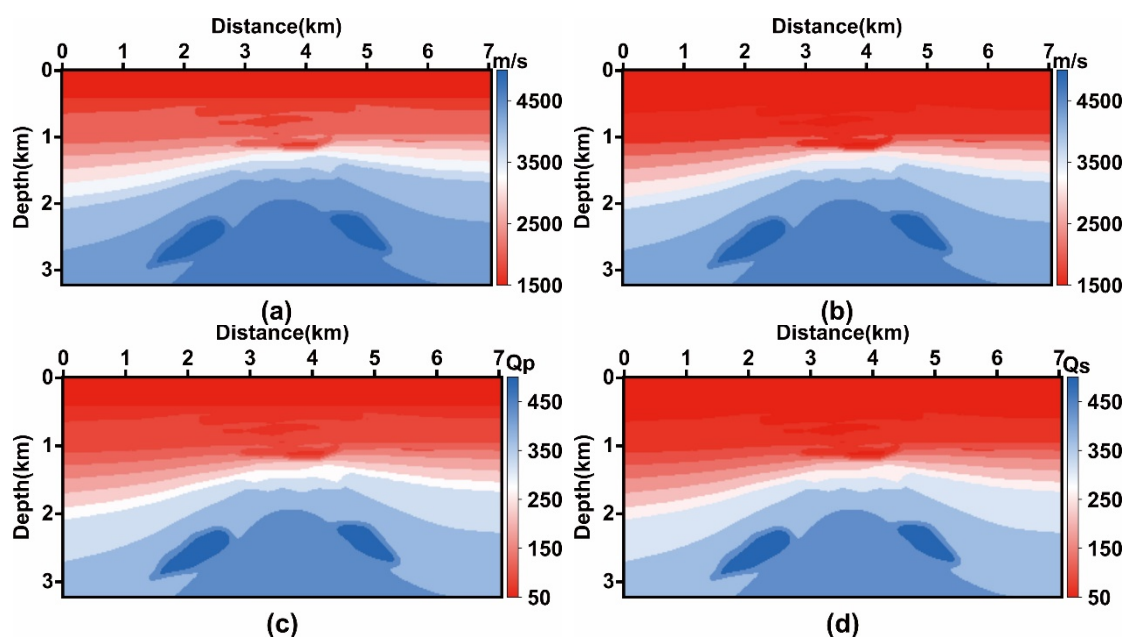


Fig. 7. 2D BP gas chimney model: (a) V_p , (b) V_s , (c) Q_p , (d) Q_s .

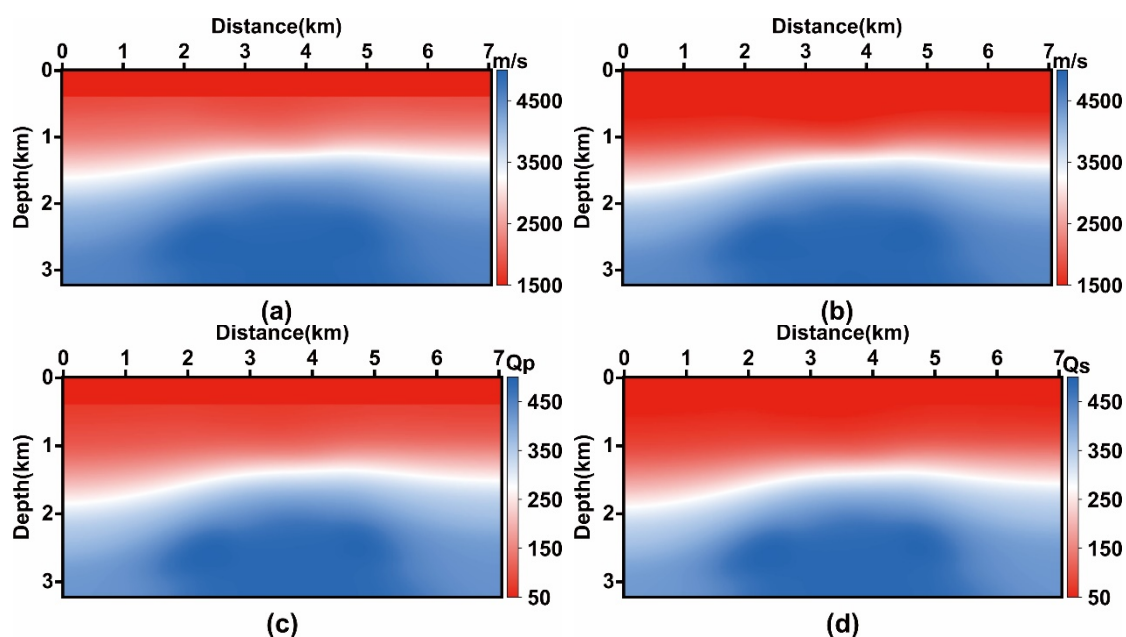


Fig. 8. Initial model: (a) V_p , (b) V_s , (c) Q_p , (d) Q_s .

In this paper, we first compare the inversion gradients of the 2D BP gas chimney model. From Fig. 9, we can know that the gradient without gradient preprocessing falls into local convergence, and the other subsurface media are difficult to get sufficient inversion. As can be seen from Fig. 10, the overall energy of the gradient after the gradient preprocessing is more average, and the other subsurface media are adequately inversion. The results of the gradient prove that the P-QEFWI method can suppress the local convergence that the gradient falls into due to the low velocity body.

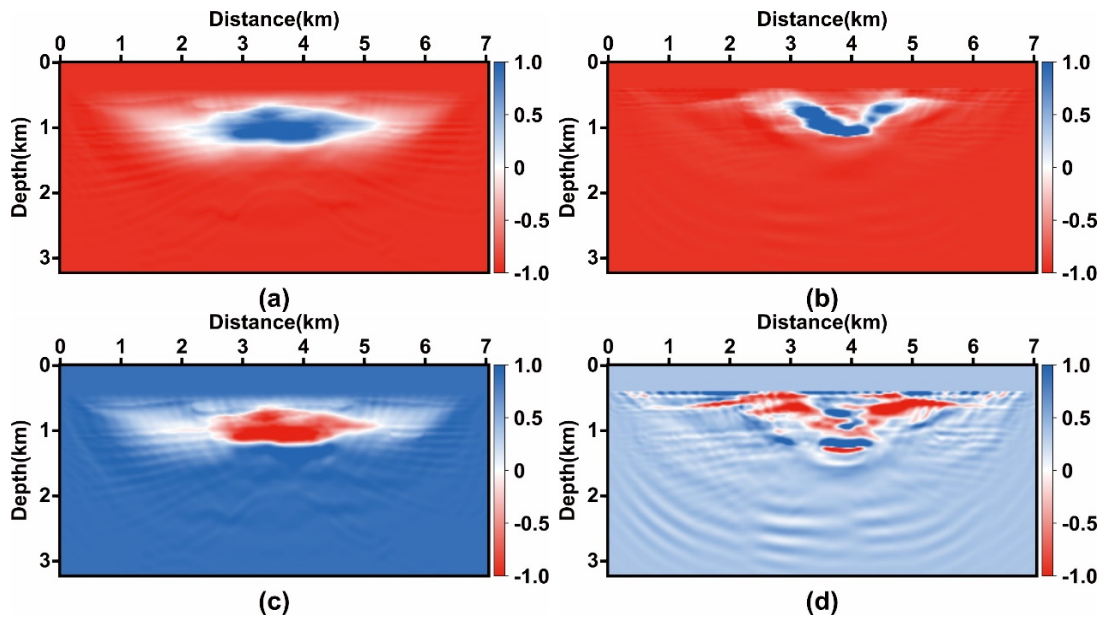


Fig. 9. Gradient without gradient preprocessing: (a) V_p , (b) V_s , (c) Q_p , (d) Q_s .

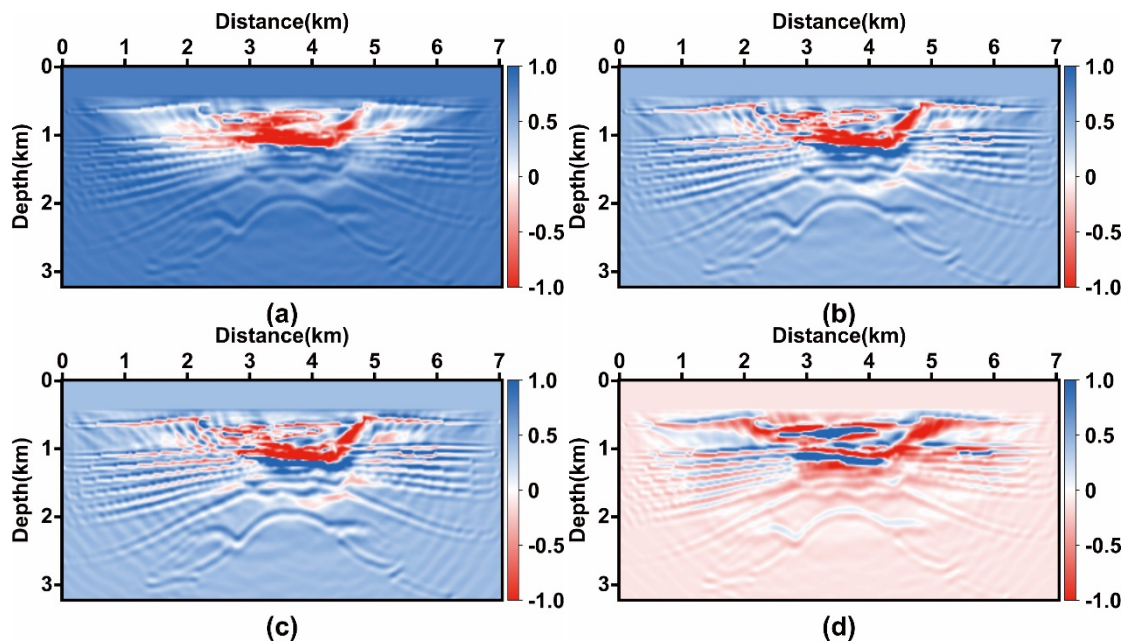


Fig. 10. Gradients after gradient preprocessing: (a) V_p , (b) V_s , (c) Q_p , (d) Q_s .

We compared the inversion results of the 2D BP gas chimney model. As can be seen from Fig. 11, V_p and V_s of the QEFWI method obtain general inversion accuracy, while Q_p and Q_s inversions have no effect due to local convergence trapped at the low velocity body. All four parameters of the P-QEFWI method obtain high inversion accuracy without local convergence trapped at the low-velocity body. The inversion results prove that the P-QEFWI method can suppress the local convergence of the gradient caused by the low-velocity body and improve the inversion accuracy of the parameters.

In this paper, we next compare the single-line results at 3.5 km. From Figs. 12-15, it can be seen that the P-QEFWI method has a small improvement in the accuracy of V_p and V_s , and the P-QEFWI method has a larger improvement in the accuracy of Q_p and Q_s . Therefore, the information obtained from Figs. 11-15 is consistent, and the method can suppress the local convergence of the gradient caught by the low velocity body and improve the accuracy of the inversion results.

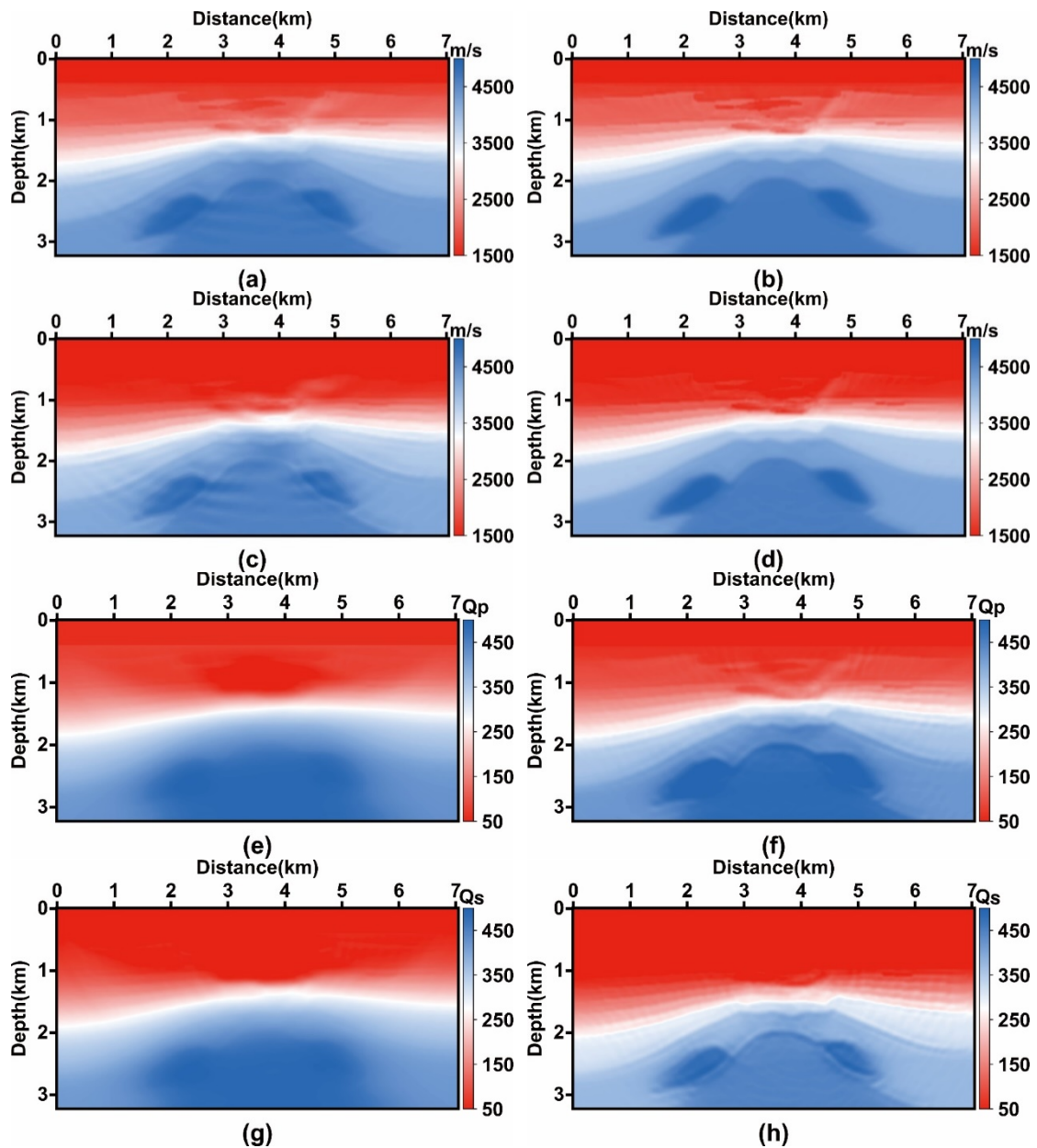


Fig. 11. Inversion results without gradient preprocessing: (a) V_p , (c) V_s , (e) Q_p , (g) Q_s ; Inversion results with gradient preprocessing: (b) V_p , (d) V_s , (f) Q_p , (h) Q_s .

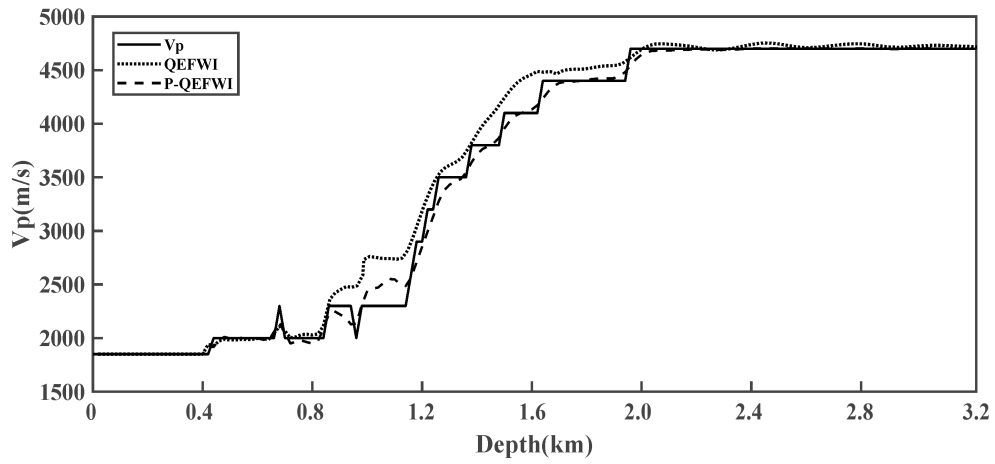


Fig. 12. V_p single line comparison at 3.5 km.

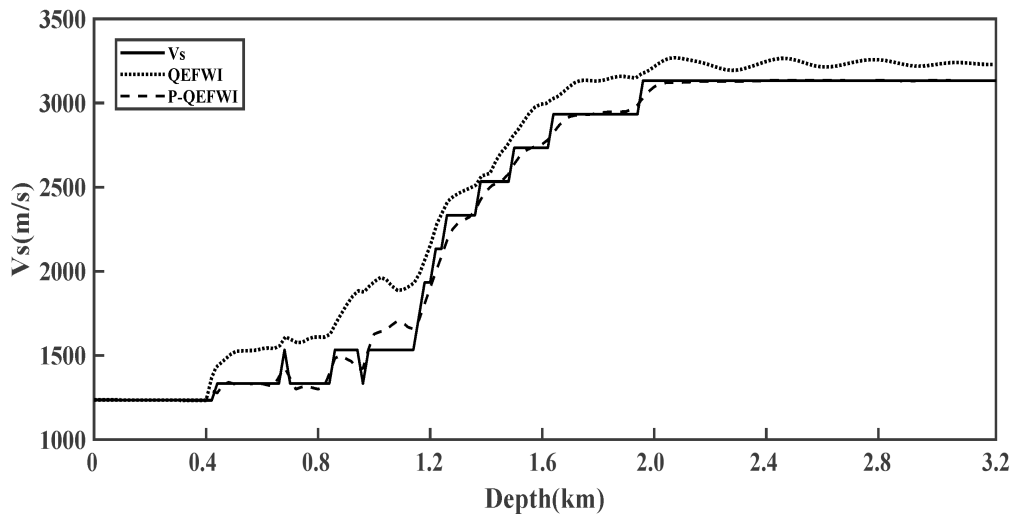


Fig. 13. V_s single line comparison at 3.5 km.

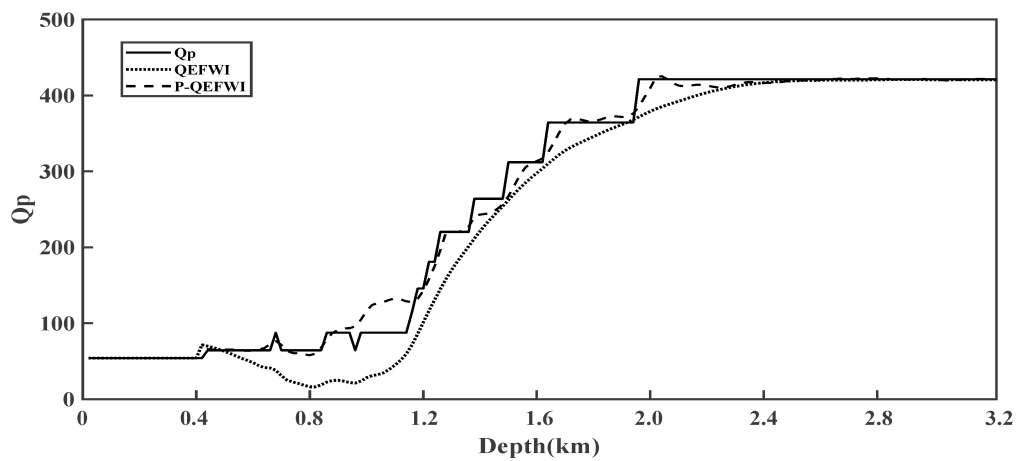


Fig. 14. Q_p single line comparison at 3.5 km.

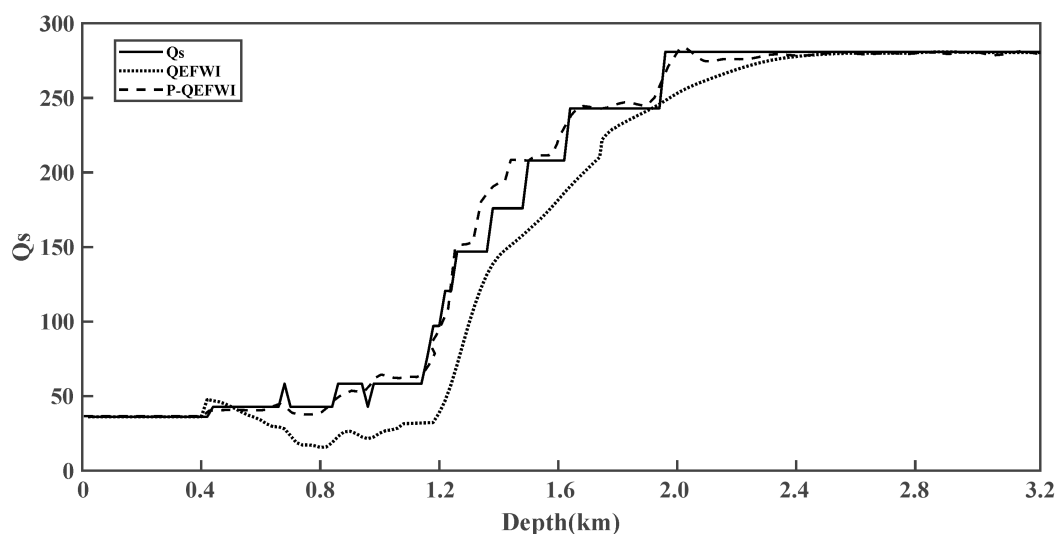


Fig. 15. Qs single line comparison at 3.5 km.

CONCLUSION

In this paper, we derive the back-propagation wavefield formulation and gradient formulation for full waveform inversion in viscoelastic media based on the Kelvin-Voigt model, and prove the correctness of the gradient formulation and wavefield back-propagation formulation of the method. Meanwhile, in viscoelastic media, the low velocity causes the gradient of full waveform inversion to fall into local convergence. Therefore, this paper adds the pseudo-Hessian operator for gradient preprocessing and derives the gradient preprocessing formula for full waveform inversion in viscoelastic media based on gradient preprocessing, which solves the problem that the inversion gradient falls into local convergence. It is proven through examples that the method can solve the problem of inversion gradient falling into local convergence caused by low-velocity bodies in full waveform inversion of viscoelastic media, and improve the accuracy of parameter inversion results.

ACKNOWLEDGEMENTS

We are grateful to the teachers and students of the Seismic Wave Propagation and Imaging Group for their help and support.

Fund project : This study is jointly funded by CNPC major science and technology project “Research on key technologies of seismic velocity modeling and imaging of deep complex high-steep structures and carbonate reservoirs in Tarim Basin” (ZD2019-183-003), National Natural Science Foundation of China “Viscoelastic parameter inversion imaging method for

deep lithologic reservoirs” (42074133), and the special fund project of basic scientific research funds of central universities “Research on seismic wave imaging method of complex anisotropic media” (19CX02056 A) National Science and Technology Major Sub-project “Research on high-precision velocity modeling and imaging method under salt” (2017ZX0532-003-002).

REFERENCES

- Alkhalifah, T., 2015. Conditioning the full-waveform inversion gradient to welcome anisotropy. *Geophysics*, 80(3): R111-R122. doi: 10.1190/geo2014-0390.1.
- Biondi, B. and Almomin, A., 2012. Tomographic full waveform inversion (TFWI) by combining full waveform inversion with wave-equation migration velocity analysis. Expanded Abstr., 82nd Ann. Internat. SEG Mtg., Las Vegas: 1074-1080.
- Bozdağ, E., Trampert, J. and Tromp, J., 2011. Misfit functions for full waveform inversion based on instantaneous phase and envelope measurements. *Geophys. J. Internat.*, 185: 845-870. doi: 10.1111/j.1365-246X.2011.04970.x.
- Choi, Y. and Alkhalifah, T., 2013. Frequency-domain waveform inversion using the phase derivative. *Geophys. J. Internat.*, 195: 1904-1916. doi: 10.1093/gji/ggt351.
- Dong, R., Cai, D.S. and Soichiro, I., 2020. Motion capture data analysis in the instantaneous frequency-domain using Hilbert-Huang transform. *Sensors*, 20: 6534. doi: 10.3390/s20226534.
- Engquist, B., Froese, B. and Yang, Y., 2016. Optimal transport for seismic full waveform inversion. *Communic. Mathemat. Sci.*, 14: 2309-2330. arXiv:1602.01540.
- Huang, C.J., Song, H.J. and Lei, W.P., 2019. Instantaneous amplitude-frequency feature extraction for rotor fault based on BEMD and Hilbert Transform. *Shock Vibrat.*, Vol. 2019: 1-19. doi:10.1155/2019/1639139.
- Huang, S., Ren, C., Li, Z.C., Gu, B.L. and Li, H.M., 2019. Full waveform inversion of multi-source elastic waves with longitudinal and transverse wave separation. *Petrol. Geophys. Explor.*, 54: 1 084-1093. doi: 10.13810/j.cnki.issn.1000-7210.2019.05.016.
- Li, Z.C., Zhang, H., Liu, Q.M. and Han, W.G., 2007. Numerical simulation of wavefield separation by high-order finite difference method with elastic wave interlacing grid. *Petrol. Geophys. Explor.*, 42: 510-515. doi: CNKI:SUN:SYDQ.0.2007-05-007.
- Luo, J.R., Wu, R.S. and Gao, F.C., 2018. Time domain full waveform inversion using instantaneous phase with damping. *J. Geophys. Engineer.*, 15: 1032-1041. doi: 10.1088/1742-2140/aaa984.
- Luo, J., Wu, R. and Gao, J., 2016. Local minima reduction of seismic envelope inversion. *Chin. J. Geophys.*, 59: 2510-2518. doi: 10.6038/cjg20160716.
- Métivier, L., Brossier, R., Méridot, Q., Oudet, E. and Virieux, J., 2016. An optimal transport approach for seismic tomography: application to 3D full waveform inversion. *Inverse Probl.*, 32: 115008. doi: 10.1088/0266-5611/32/11/115008/meta.
- Mora, P., 1987. Nonlinear two-dimensional elastic inversion of multi-offset seismic data. *Geophysics*, 52: 1211-1228. doi: 10.1190/1.1442384.
- Pratt, R.G., Shin, C. and Hick, G.J., 1998. Gauss-Newton and full Newton methods in frequency-space seismic waveform inversion. *Geophys. J. Internat.*, 133: 341-362. doi: 10.1046/j.1365-246X.1998.00498.x.
- Raknes, E. and Arntsen, B., 2014. Strategies for elastic full waveform inversion. Expanded Abstr., 84th Ann. Internat. SEG Mtg., Denver: 1222-1226.
- Ren, Z.M. and Liu, Y., 2016. A hierarchical elastic full-waveform inversion scheme based on wavefield separation and the multistep-length approach. *Geophysics*, 81(3): R99-R123. doi: 10.1190/geo2015-0431.1
- Shah, N.K., Warner, M.R., Washbourne, J.K., Guasch, L. and Umpleby, A., 2012. A phase-unwrapped solution for overcoming a poor starting model in full-wavefield inversion. Extended Abstr., 74th EAGE Conf., Copenhagen: P014.
- Shin, C. and Ho, C.Y., 2009. Waveform inversion in the Laplace-Fourier domain. *Geophys. J. Internat.*, 177: 1067-1079. doi: 10.1111/j.1365-246X.2009.04102.x.

- Tarantola, A., 1987. Inverse problem theory: Methods for data fitting and model parameter estimation. Elsevier Science Publ. Co., Inc., New York.
- Tristan, V.L. and Felix, J.H., 2013. Mitigating local minima in full-waveform inversion by expanding the search space. *Geophys. J. Internat.*, 195: 661-667. doi: 10.1093/gji/ggt258.
- Wang, B., Jakobsen, M., Wu, R.S., Lu, W. and Chen, X., 2017. Accurate and efficient velocity estimation using Transmission matrix formalism based on the domain decomposition method. *Inverse Probl.*, 33: 035002. doi: 10.1088/1361-6420/aa5998.
- Wang, T.F. and Cheng, J.B., 2017. Elastic full waveform inversion based on mode decomposition: The approach and mechanism. *Geophys. J. Internat.*, 209: 606-622. doi:10.1093/gji/ggx038.
- Warner, M., Lluís, G. and Gang, Y., 2015. Adaptive waveform inversion-FWI without cycle skipping. Expanded Abstr., 85th Ann. Internat. SEG Mtg., New Orleans: 11-14.
- Wu, R.S., Luo, J.R. and Wu, B.Y., 2014. Seismic envelope inversion and modulation signal model. *Geophysics*, 79(10): WA13-WA24. doi: 10.1190/geo2013-0294.1.
- Xu, Y.P., Ren, Z.M., Li Z.C., Liu, C., He, Z.L. and Chen, J.M., 2020. First-order approximate instantaneous frequency time domain acoustic full waveform inversion. *Petrol. Geophys. Explor.*, 55: 1029-1038. doi: 10.13810/j.cnki.issn.1000-7210.2020.05.011.
- Yang, Y., Engquist, B., Sun, J. and Hamfeldt, B.F., 2018. Application of optimal transport and the quadratic Wasserstein metric to full-waveform inversion. *Geophysics*, 83(1): R43-R62. doi:10.1190/geo2016-0663.1.